Large renal lymphoma in a patient with horseshoe kidney: A case report

FRANCESCO IOVINO[1], FEDERICO MARIA MONGARDINI[1], GIOVANNI BALESTRUCCI[2], ALFONSO REGGINELLI[2], ANDREA RONCHI[3], MARIA GIOVANNA FERRARA[2], SIMONA PARISI[4], CLAUDIO GAMBARDELLA[4], FRANCESCO SAVERIO LUCIDO[4], SALVATORE TOLONE[4], ROBERTO RUGGIERO[4] and LUDOVICO DOCIMO[4]

Departments of [1]Translational Medical Sciences, [2]Precision Medicine, [3]Mental and Physical Health and Preventive Medicine, and [4]Advanced Medical and Surgical Sciences, School of Medicine, University of Campania Luigi Vanvitelli, I-80131 Naples, Italy

Received June 23, 2023; Accepted September 28, 2023

DOI: 10.3892/ol.2023.14180

Abstract. Horseshoe kidney (HSK) is the most common renal fusion anomaly. It frequently consists of kidney fusion in the lower pole across the midline and occurs during embryogenesis. The incidence of malignancies in HSKs can be 3-4 times higher than that in normal kidneys. A 69-year-old man with a voluminous right kidney neoplasm in HSK and a single omolateral axillary lymphadenopathy underwent complete excision of right axillary lymphadenopathy and ultrasound-guided percutaneous biopsy of the right kidney expansive lesion. The diagnosis of non-Hodgkin's B cell lymphoma both in HSK and right axilla was made. We report this case to raise awareness among physicians regarding the importance of a correct clinical evaluation and diagnostic workup so as to avoid surgery, which is not easy and without complications, in patients with this kidney anomaly. Primary renal lymphoma should also be included among possible neoplasms of HSK. Renal biopsy should always be recommended in cases where atypical findings are obtained from imaging techniques and when its outcome can impact clinical decision-making. In the present case, biopsy was performed, and thus, nephrectomy was avoided and specific medical therapy was quickly started.

Introduction

Horseshoe kidney (HSK) is the most common renal fusion anomaly, with a prevalence of 0.25% among the general population and is more common in males (1,2). It frequently consists of kidney fusion in the lower pole across the midline and occurs during embryogenesis (2). Furthermore, this rare entity can be detected as an incidentaloma during a diagnostic assessment for other reasons or otherwise due to urogenital disorders. The incidence of malignancies in HSKs can be 3-4 times higher than that in normal kidneys (1-3). Renal cell carcinoma (RCC) is the most frequent malignancy in patients with HSK (4-6). B cell lymphoma in a HSK has not yet been reported in the literature, according to a search performed in both the PubMed (7) and Google Scholar databases (8), using 'horseshoe kidney' and 'B cell lymphoma' as key words. Therefore, to the best of our knowledge, the present report describes the first case of B cell lymphoma in a HSK to raise awareness among physicians regarding the importance of a correct clinical evaluation and diagnostic workup to avoid surgery, which is not easy and without complications (9), in patients with this kidney anomaly.

Case report

A 69-year-old man was referred to the General Surgery Division of University of Campania Luigi Vanvitelli (Naples, Italy) in January 2023 due to a voluminous right kidney neoplasm, previously detected on abdominal ultrasound. Ultrasound revealed a voluminous neoplasm measuring 8x6 cm in the right kidney, which was markedly vascularized on Doppler analysis. A HSK with inferior pole fusion was also reported. The neoplasm occupied the renal pelvis and caused calico-pielic dilation. The patient had no urinary symptoms and was unaware of their kidney anomaly. Routine laboratory tests were normal, except RBC, HCT, PLT, PCT, phosphorous, creatine phosphokinase and transferrin that were lower than the normal range, and MCH, bilirubin total, direct and indirect, and ferritin that were higher than the normal range; renal function also showed no signs of impairment (Table I). On clinical examination, a mass in the right flank was palpated, occupying the entire right hemi-abdomen. No abnormalities were found in the chest except for the presence of a single, painless, mobile, enlarged (diameter, 3 cm)

Correspondence to: Professor Francesco Iovino, Department of Translational Medical Sciences, School of Medicine, University of Campania Luigi Vanvitelli, Via Sergio Pansini 5, I-80131 Naples, Italy
E-mail: francesco.iovino@unicampania.it

Key words: horseshoe kidney, non-Hodgkin's lymphoma, kidney biopsy

Table I. Laboratory analysis.

Parameter	Patient value	Normal value
WBC, x10^3/μl	7.60	4.50-11.00
Neutrophils, x10^3/μl	4.72	2.20-7.50
Lymphocytes, x10^3/μl	2.23	1.00-5.00
Monocytes, x10^3/μl	0.70	0.16-1.00
Eosinophils, x10^3/μl	0.12	0.0-0.60
Basophils, x10^3/μl	0.04	0.0-0.20
RBC, x10^6/μl	4.39	4.50-6.00
HGB, g/dl	13.92	13.00-17.50
HCT, %	39.84	42-51
MCV, fL	90.70	82-96
MCH, pg	31.70	27-31
MCHC, g/dl	34.92	31-36
PLT, x10^3/μl	121	150-450
MPV, fL	11.80	7.40-12.50
PCT, %	0.14	0.19-0.38
Glucose, mg/dl	70	70-100
Urea, mg/dl	40	10-50
Creatinine, mg/dl	1.13	0.67-1.17
Uric acid, mg/dl	5.80	3.40-7.00
Sodium, mEq/l	142	135-146
Potassium, mEq/l	3.90	3.50-5.30
Chlorine, mEq/l	106	98-111
Albumin, g/dl	4.50	3.50-5.50
Total protein, g/dl	6.90	6.60-8.70
Cholesterol tot., mg/dl	124	60-200
Cholesterol HDL, mg/dl	52	>35
Cholesterol LDL, mg/dl	56	10-129
Triglycerides, mg/dl	80	20-175
Cholinesterase, U/l	7498	5320-12920
GGT, U/l	15	8-61
ALT-GPT, U/l	15	5-41
AST-GOT, U/l	20	0-34
Bilirubin tot., mg/dl	1.49	<1.2
Bilirubin dir., mg/dl	0.56	<0.30
Bilirubin indir., mg/dl	0.93	<0.75
Phosphorus, mg/dl	2.50	2.70-4.50
Calcium, mg/dl	9.50	8.60-10.20
Amylase, U/l	72	28-100
Lipase, U/l	46	13-78
Alkaline phosphatase, U/l	128	40-129
Creatine phosphokinase, U/l	43	60-190
LDH, U/l	198	120-240
Iron, μg/ml	107	59-158
Ferritin, ng/ml	430	30-400
Transferrin, mg/dl	190	191-337
PT, sec	10.50	9-13
INR	0.91	0.80-1.20
aPTT, sec	33.40	24-38
Fibrinogen, mg/dl	236	200-400

ALT-GPT, alanine transaminase-glutamic pyruvic transaminase; aPTT, activated partial thromboplastin time; AST-GOT, aspartate aminotransferase-glutamic oxaloacetic transaminase; dir., direct; GGT, γ-glutamyl transferase; HCT, hematocrit; HDL, high-density lipoprotein; HGB, hemoglobin; INR, international normalized ratio; LDH, lactate dehydrogenase; LDL, low-density lipoprotein; MCH, mean corpuscular hemoglobin; MCHC, mean corpuscular hemoglobin concentration; MCV, mean corpuscular volume; MPV, mean platelet volume; PCT, procalcitonin; PLT, platelet count; PT, prothrombin time; RBC, red blood cell; tot., total; indir., indirect; WBC, white blood cell.

lymph node in the right axilla. There were no other enlarged superficial lymph nodes. As part of the radiological work-up, a total body CT scan was performed, which revealed a single right axillary lymphadenopathy (37x28 mm; Fig. 1) and renal inferior pole fusion consistent with a HSK, with a hypodense right renal neoplasm (109x108x92 mm; Fig. 2) within its

Figure 1. Contrast-enhanced CT scan, portal phase. Chest CT scan showing lymphadenopathy in the right axilla (white asterisk; R: right).

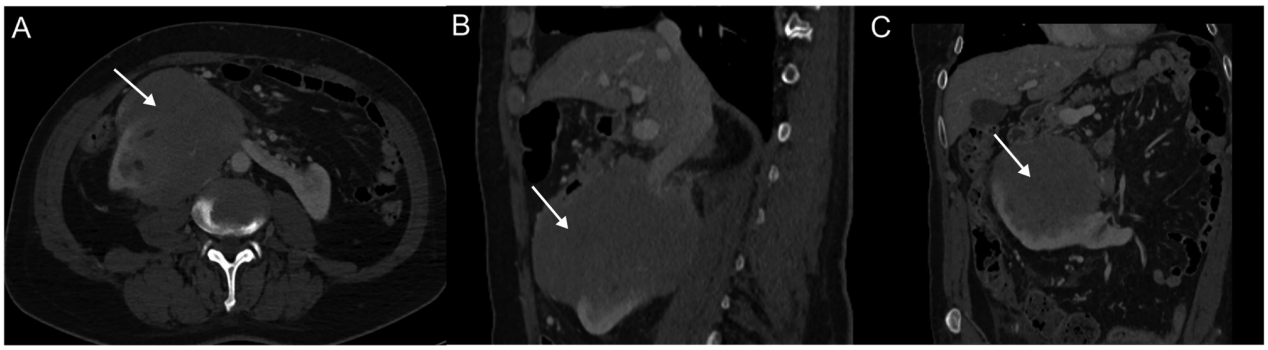

Figure 2. Contrast-enhanced CT scan, portal phase. (A) Axial, (B) sagittal and (C) coronal plane. Abdominal CT scans showing the presence of a large mass (arrow) located in the right side of the horseshoe kidney. The mass exhibited non-homogeneous enhancement, less than the normal kidney parenchyma.

context. This formation involved a large part of the right hemi-abdomen resulting in anterior duodenum displacement and posterior dislocation with compression of the inferior vena cava (Fig. 3). No other abnormalities were found. Abdomen MRI confirmed the large renal formation (Fig. 4) incorporating the pielic sinus and the mesorenal parenchyma, indissociable from the duodenal fold, despite no evident signs of invasion. No abdominopelvic lymphadenopathies were described. Absence of a well-defined capsule, preservation of the 'reniform' appearance and indistinct margins, as well as high diffusion restriction were reported on MRI. A transduodenal endoscopic ultrasound was performed to evaluate infiltration of the duodenal wall by the neoplasm. This indicated only duodenal compression and dislocation but no infiltration (Fig. 5).

The patient underwent complete excision of the right axillary lymphadenopathy and ultrasound-guided percutaneous biopsy of the right kidney expansive lesion. The procedures were performed without complications. The samples were formalin fixed and paraffin embedded, fixation was obtained by leaving the sample in formalin (concentration 10%) for 48 h at room temperature. 7 μm-thick slides were cut and strained by hematoxylin and eosin (40 min at room temperature). A light microscope was used for histological examination. Histological examination showed renal parenchyma partially effaced by a lymphoid population (Fig. 6A) with nuclear crushing, mainly constituted by small lymphocytes (Fig. 6B).

Figure 3. Contrast-enhanced CT scan, portal phase. Abdominal CT scan showing the compression of the third duodenal portion (as previously shown by endoscopic ultrasound), without a clear surgical cleavage plane between its wall and the large renal mass (black circle). Compression of the inferior vena cava (white asterisk) by the lesion can also be seen.

Immunohistochemistry was performed on formalin fixed and paraffin embedded 4μm thick tissue sections (fixative concentration: 10% formalin; fixative temperature: room temperature; duration: 48 h). Immunohistochemistry was performed automatically on BenchMark Ultra platform (Ventana Medical Systems), according to the manufacturer's instructions. Antigen retrieval was performed by using Ultra CC1 for 36 min at

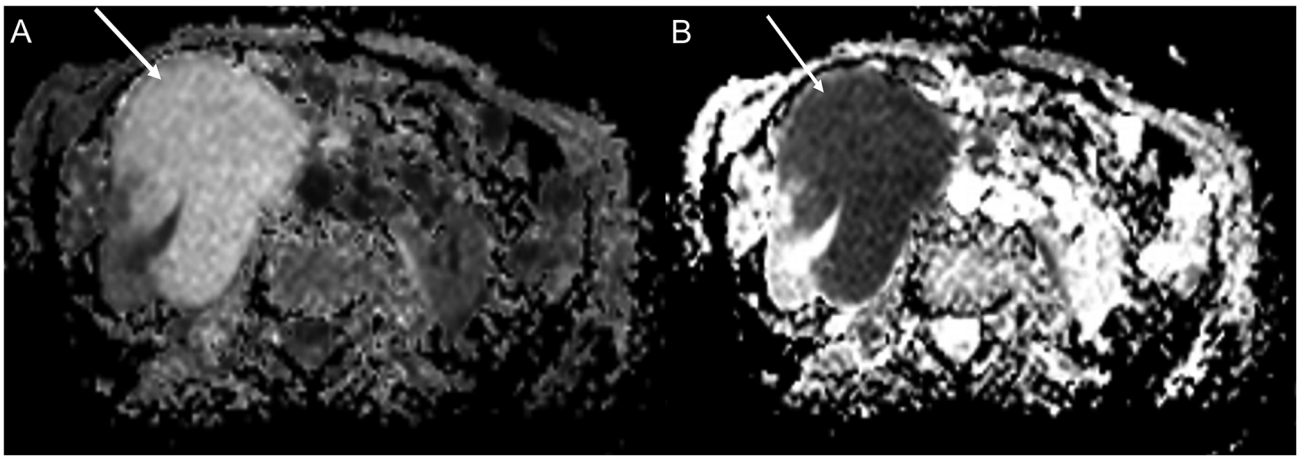

Figure 4. MRI. MRI scan showing a high restriction of lesion's diffusivity (arrow) on (A) DWI, confirmed by the corresponding (B) ADC map. ADC, apparent diffusion coefficient; DWI, diffusion-weighted imaging.

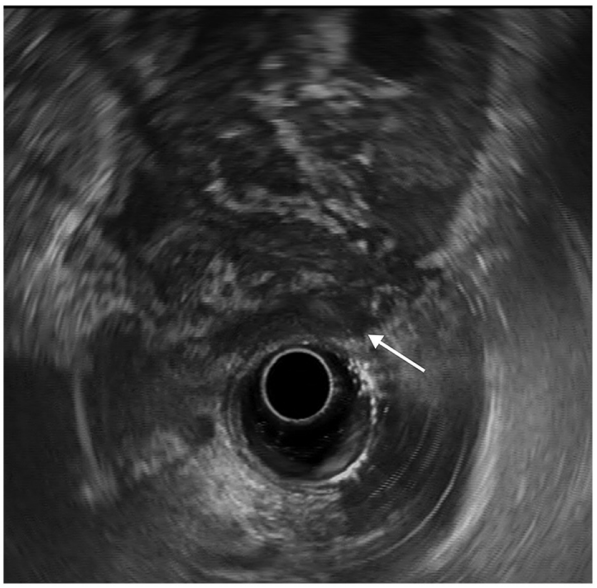

Figure 5. EUS. Trans-duodenal EUS showing duodenal compression and dislocation by the large renal mass (arrow). EUS, endoscopic ultrasound.

95˚C. Endogenous peroxides and proteins blocking was done in the platform using Inhibitor CM, ready to use dilution, 37˚C, 4 min. Tissues sections were incubated with the monoclonal antibodies (Ventana Medical Systems) for 32 min at 37˚C (dilution: ready to use). Immunoreactivity was visualized using an OptiView DAB IHC detection kit (Ventana Medical Systems, cat. no. 760-700), incubation at 37˚C for 8 min, and then counterstained with Hematoxylin II and Bluing Reagent for 8 min and 4 min respectively, at the room temperature. We used the following antibodies: CD20 (Ventana - Roche, cat. no. 760-2531), Bcl6 (Ventana-Roche, cat. no. 760-4241), Bcl2 (Ventana-Roche, cat. no. 790-4464), CD3 (Ventana-Roche, cat. no. 790-4341), CD10 (Ventana-Roche, cat. no. 790-4506), Cyclin D1 (Ventana-Roche, cat. no. 790-4508), IgD (Ventana - Roche, cat. no. 760-4444), CD21 (Ventana-Roche, cat. no. 760-4438), CD23 (Ventana-Roche, cat. no. 790-4408), Ki67 (Ventana-Roche, cat. no. 790-4286). Secondary antibody (ready to use, Ventana-Roche, cat. no. 760-099, conjugate HRP multimer, temperature 36˚C, incubation 8 min. A light microscope was used for the interpretation.

Immunohistochemistry indicated positivity for CD20 (Fig. 6C) and Bcl6 (Fig. 6D). A diagnosis of non-Hodgkin's B-cell lymphoma consistent with grade G1/G2 follicular lymphoma was made according to World Health Organization10). Definitive histological assessment of the axillary lymph node also revealed a follicular arranged lymphoid population (Fig. 7A) constituted by centrocytes and centroblasts (Fig. 7B), positive staining for CD20 (Fig. 7C) and Bcl6 (Fig. 7D) in immunohistochemistry, and negative staining for Bcl2 (Fig. 7E), CD3, CD10, CD5, Cyclin D1, IgD, CD21 and CD23 (data not shown). The proliferation index (Ki67) was 15% (Fig. 7F). Therefore, a conclusive diagnosis of World Health Organization grade G1/G2 follicular lymphoma with follicular pattern was made (10). Fluorescence *in situ* hybridization did not detect BCL2 genetic rearrangements in either biopsy (data not shown). FISH assay was performed on 4-μm-thick sections cut from each of the formalin-fixed paraffin-embedded biopsy specimens using the BOND FISH kit (Leica Biosystems, Newcastle Upon Tyne, UK) on the automated BOND system (Leica Biosystems) according to the manufacturer's instructions. FISH automatic protocol includes the following steps: deparaffinization of sections by Bond dewax solution at 96˚C for 1 min; pretreatment by BOND Epitope Retrieval Solution at 76˚C for 25 min and at 37˚C for 12 min, and enzymatic pretreatment by BOND Enzyme Pre-treatment Kit (enzyme dilution 1:100) at 37˚C for 35 min. Denaturation and hybridization of the probe were performed on the automated BOND system (Leica Biosystems): 75˚C for 5 min for the denaturation process and 37˚C for 17 h for the hybridization of BCL2 probes. The used probe was the commercially available ready-for-use probe ZytoLight SPEC BCL2 Dual Color Break Apart Probe (ZytoVision) that is composed as follows: ZyGreen (excitation 503 nm/emission 528 nm) labeled polynucleotides (~10 ng/μl), which target sequences mapping in 18q21.3 (chr18:60,046,152-60,589,273) proximal to the BCL2 breakpoint region and ZyOrange (excitation 547 nm/emission 572 nm) labeled polynucleotides (~4.5 ng/μl), which target sequences mapping in 18q21.33-q22.1 (chr18:60,994,528-61,658,503) distal to the BCL2 breakpoint

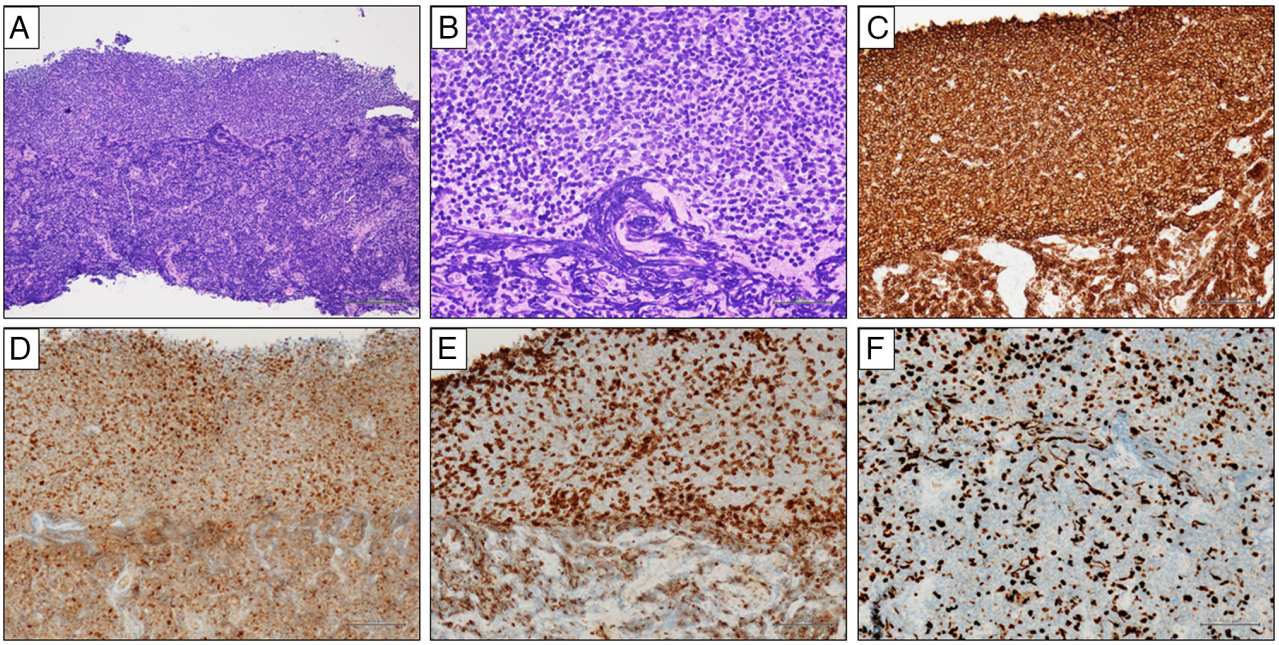

Figure 6. Histological findings of renal biopsy. (A) Biopsy showed a diffuse lymphoid population with nuclear crushing (H&E stain; original magnification, x40). (B) The lymphoid population comprised small lymphocytes (H&E stain; original magnification, x200). (C) Immunohistochemistry showed positivity for CD20 (original magnification, x200) and (D) Bcl6 (Bcl6 immunostain; original magnification, x200). (E) A T-cell reactive population was present in the background as demonstrated by CD3 immunohistochemistry (CD3 immunostain; original magnification, x200). (F) The proliferation index (Ki67) was ~15% (Ki67 immunostain; original magnification, x400).

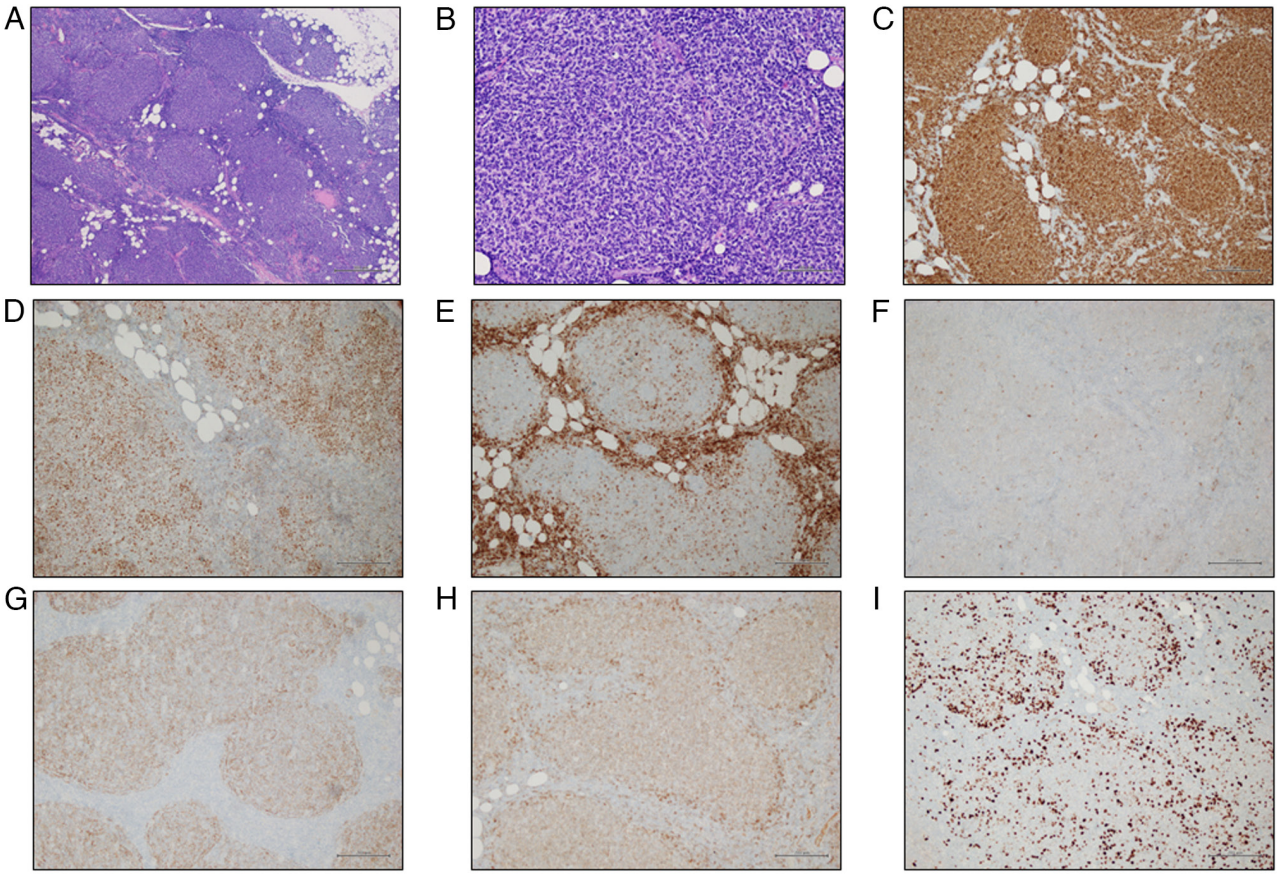

Figure 7. Histological findings of lymph node biopsy. (A) The lymph node parenchyma was replaced by a lymphoid population arranged in nodules (H&E stain; original magnification, x40). (B) The lymphoid population was composed of many centrocytes and few centroblasts (H&E stain; original magnification, x200). Immunohistochemically, the population was positive for (C) CD20 and (D) Bcl6 (Bcl6 immunostain; original magnification, x100), and negative for (E) Bcl2 (Bcl2 immunostain; original magnification, x100) and (F) CD10 (CD10 immunostain; original magnification, x100). The neoplastic follicles were (G) partially supported by a meshwork of CD21-positive follicular dendritic cells (CD21 immunostain; original magnification, x100), and (H) partially surrounded by a thin IgD-positive mantle cell layer (IgD immunostain; original magnification, x100). (I) The proliferation index (Ki67) was ~15% (magnification, x100).

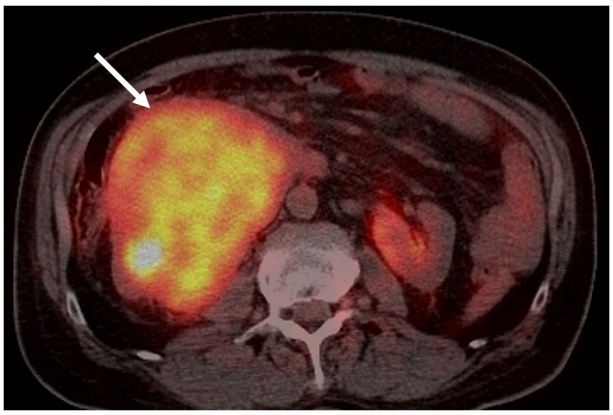

Figure 8. PET, fusion image. Abdominal PET image showing a marked 'avidity' of tumor cells for the radiotracer within the large renal lesion (arrow). PET, positron emission tomography.

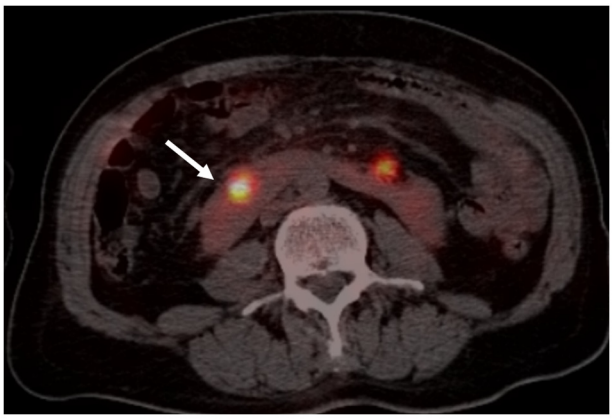

Figure 9. Follow-up PET, fusion image. Follow-up abdominal PET image showing the kidney after treatment, without any pathological uptake (arrow). The mass previously observed was not detected as the right part of the horseshoe kidney had a regular appearance. PET, positron emission tomography.

region. The slides were then washed to reduce non-specific hybridization of nucleic acid probes by Post Hybridization Wash containing formamide (<50%) at 48˚C for 4 min. The slides were washed with purified water, air-dried, and dehydrated in ascending grades of alcohol. Lastly, 10 μl of DAPI was applied on the slides. FISH interpretation was performed with the automated fluorescence microscope Leica DM5500 B (Leica Biosystems) using the filter ET-D/O/G for double Spectrum Green plus Spectrum Orange. FISH for BCL2 locus rearrangements is considered positive in relation to the presence of a break-apart pattern with one fusion signal and two separated orange and green signals in more than 15% of the cells analyzed. In our case, FISH signals were counted in ≥100 nonoverlapping intact nuclei and no break-apart pattern was observed. Finally, 18-fluorodeoxyglucose (18-FDG) positron emission tomography (PET)-CT showed an isolated, large area of tracer accumulation (maximum standardized uptake value, 20.1) in the right HSK section (Fig. 8). The patient was started on chemo-immunotherapy, according to a standard protocol (1,000 mg Gazyvaro administered over day 1, 8, 15 of cycle 1 + 90 mg/mq bendamustine on day 1, 2 of the same cycle; the planned dose of 1,000 mg Gazyvaro on day 1 + 90 mg/mq bendamustine on day 1,2 had been administered for additional five cycles every 28 days; followed by 1,000 mg Gazyvaro maintenance every 2 months for 2 years or until disease progression). At the end of the treatment, in May 2023, 18-FDG PET-CT was performed, demonstrating a complete remission of the disease in the right kidney without any other suspicion of disease (Fig. 9). Currently, the patient is in good clinical condition, undergoing maintenance therapy with Gazyvaro and follow-up with 18-FDG PET-CT every six months for two years, and then once a year for five years.

Discussion

Primary renal non-Hodgkin's lymphoma is a rare disease and only a few cases have been reported in the literature (6,11-15). Furthermore, no case reports describing the association between HSK and renal lymphoma have been documented.

Mendelson *et al* (16) reported a case of HSK anomaly mimicking an isolated preaortic lymphadenopathy on ultrasonographic imaging; in case of diagnostic doubt, an urogram or uro-CT scan should be considered in order to avoid misdiagnosis and to improve the resolution of the anatomical structures.

A higher incidence of renal cancer has been reported in individuals with a HSK than in the general population (4-6). The main cause is considered to be chronic inflammation resulting from difficulty urinating due to renal abnormalities, such as ureteropelvic obstruction, lithiasis and infections (17). The present patient had no clinical and radiological signs of urinary output impairment or urinary infection despite the presence of a large tumor. Therefore, we hypothesized that the pathogenetic mechanism and growth modality of lymphoma are different from those of renal cancer. When considering solid renal masses or cystic masses with solid components, the initial assumption often is that it may be a malignant neoplasm of the kidney (18). In the past, the treatment of choice usually involved radical nephrectomy; however, over the years, there has been a shift towards partial nephrectomy or a more conservative approach (19). In the present case, due to the careful use of imaging techniques (mainly CT and MRI), characteristics of a possible renal lymphoma were recognized in the mass, including the absence of a well-defined capsule, preservation of the 'reniform' appearance and indistinct margins (20), as well as high diffusion restriction on MRI. These features, combined with the presence of the right axillary bulky lymphadenopathy, raised suspicion of renal lymphoma as the primary hypothesis, and thus, a biopsy was performed, leading to a definitive diagnosis, while preserving the kidney. We hypothesized that renal biopsy should always be recommended when its outcome can impact clinical decision-making, especially because HSK surgery is not easy and without complications. Consequently, biopsy is warranted to distinguish between transitional cell carcinoma and RCC, to discriminate RCC from lymphoma or metastases, to differentiate malignancy from inflammatory conditions, and to acquire histological information in patients with metastatic disease (21).

In conclusion, HSK can be associated with several renal tumors, such as transitional cell carcinoma, Wilms' tumor, nephroblastoma, carcinoid tumors, sarcoma and oncocytoma (6). To the best of our knowledge, B cell non-Hodgkin's lymphoma in a HSK has never been described in the literature. The present experience suggests that primary renal lymphoma should also be included among the possible neoplasms of the HSK. A renal

biopsy should be performed before surgery in cases where atypical findings are obtained from imaging techniques. In the present case, biopsy was performed, and thus, nephrectomy was avoided and specific medical therapy was quickly initiated.

Acknowledgements

Not applicable.

Funding

No funding was received.

Availability of data and materials

All data generated or analyzed during this study are included in this published article.

Authors' contributions

FI, FMM, ARo, GB conceived and design the study. FI, ARe, RR, FSL, LD, MGF, CG, SP, ST participated in the analysis and interpretation of the data. FI, FMM, CG participated in the drafting and editing of the manuscript. GB, SP, FSL, ST constructed figures and tables. FI, FMM, GB, Are, Aro, MGF, SP, CG, FSL, ST, RR and LD confirm the authenticity of all the raw data. All authors read and approved the final version of the manuscript.

Ethics approval and consent to participate

Not applicable.

Patient consent for publication

The patient provided written informed consent for the publication of their data in this case report.

Competing interests

The authors declare that they have no competing interests.

References

1. Schiappacasse G, Aguirre J, Soffia P, Silva CS and Zilleruelo N: CT findings of the main pathological conditions associated with horseshoe kidneys. Br J Radiol 88: 20140456, 2015.
2. Humphries A, Speroni S, Eden K, Nolan M, Gilbert C and McNamara J: Horseshoe kidney: Morphologic features, embryologic and genetic etiologies, and surgical implications. Clin Anat 36: 1081-1088, 2023.
3. Kang M, Kim YC, Lee H, Kim DK, Oh KH, Joo KW, Kim YS, Chin HJ and Han SS: Renal outcomes in adult patients with horseshoe kidney. Nephrol Dial Transplant 36: 498-503, 2021.
4. Roussel E, Tasso G, Campi R, Kriegmair MC, Kara Ö, Klatte T, Capitanio U, Bertolo R, Ingels A, Erdem S, *et al*: Surgical management and outcomes of renal tumors arising from horseshoe kidneys: Results from an international multicenter collaboration. Eur Urol 79: 133-140, 2021.
5. Rivera F, Caparrós G, Vozmediano C, Bennouna M, Anaya S, Sánchez de la Nieta MD, García Rojo M and Blanco J: Riñón «en herradura», adenocarcinoma renal y síndrome nefrótico ('Horseshoe kidney', renal adenocarcinoma and nephrotic syndrome). Nefrologia 30: 596-598, 2010 (In Spanish).
6. Rubio Briones J, Regalado Pareja R, Sánchez Martín F, Chéchile Toniolo G, Huguet Pérez J and Villavicencio Mavrich H: Incidence of tumoral pathology in horseshoe kidneys. Eur Urol 33: 175-179, 1998.
7. https://pubmed.ncbi.nlm.nih.gov/
8. https://scholar.google.com/
9. Kandel LB, McCullough DL, Harrison LH, Woodruff RD, Ahl ET Jr and Munitz HA: Primary renal lymphoma: Does it exist? Cancer 60: 386-391, 1987.
10. Turner JJ, Hughes AM, Kricker A, Milliken S, Grulich A, Kaldor J and Armstrong B: WHO non-Hodgkin's lymphoma classification by criterion-based report review followed by targeted pathology review: An effective strategy for epidemiology studies. Cancer Epidemiol Biomarkers Prev 14: 2213-2219, 2005.
11. Yasunaga Y, Hoshida Y, Hashimoto M, Miki T, Okuyama A and Aozasa K: Malignant lymphoma of the kidney. J Surg Oncol 64: 207-211, 1997.
12. Farrow GM, Harrison EG and Utz DC: Sarcomas and sarcomatoid and mixed malignant tumors of the kidney in adults-part 11. Cancer 22: 551-555, 1968.
13. Freeman C, Berg JW and Cutler SJ: Occurrence and prognosis of extranodal lymphomas. Cancer 29: 252-260, 1972.
14. Bokhari SRA, Inayat F, Bokhari MR and Mansoor A: Primary renal lymphoma: A comprehensive review of the pathophysiology, clinical presentation, imaging features, management and prognosis. BMJ Case Rep 13: e235076, 2020.
15. Parsonnet J, Hansen S, Rodriguez L, Gelb AB, Warnke RA, Jellum E, Orentreich N, Vogelman JH and Friedman GD: Helicobacter pylori infection and gastric lymphoma. N Engl Med 330: 1267-1271, 1994.
16. Mendelson DS, Mitty HA, Janus C and Cohen BA: Horseshoe kidney mimicking adenopathy. Urol Radiol 5: 121-122, 1983.
17. Kawada S, Ichikawa T, Koizumi J, Hashimoto J, Endo J, Hashida K, Yamamuro H, Nomoto T, Sakamoto Y and Imai Y: Assessment of renal shape of horseshoe kidney with multidetector row CT in adult patients: Relationship between urolithiasis and renal isthmus. Tokai J Exp Clin Med 38: 159-166, 2013.
18. Pierorazio PM, Johnson MH, Patel HD, Sozio SM, Sharma R, Iyoha E, Bass EB and Allaf ME: Management of renal masses and localized renal cancer: Systematic review and meta-analysis. J Urol 196: 989-999, 2016.
19. Morrison JC, Launer BM, Barqawi ZA and Kim SP: Surgical management of the localized renal mass: Risk and benefit trade-offs and surgical approach considerations. AME Med J 6, 2020.
20. Nicolau C, Antunes N, Paño B and Sebastia C: Imaging characterization of renal masses. Medicina (Kaunas) 57: 51, 2021.
21. Ljungberg B, Albiges L, Abu-Ghanem Y, Bensalah K, Dabestani S, Fernández-Pello S, Giles RH, Hofmann F, Hora M, Kuczyk MA, *et al*: European association of urology guidelines on renal cell carcinoma: The 2019 update. Eur Urol 75: 799-810, 2019.